Generation and Detection of Single Metal Nanoparticles Using Scanning Electrochemical Microscopy Techniques†

Ran Tel-Vered and Allen J. Bard*

Department of Chemistry and Biochemistry and the Center for Nano and Molecular Science and Technology, The University of Texas at Austin, Austin, Texas 78712

Received: July 13, 2006; In Final Form: September 15, 2006

Different pathways towards the generation and detection of a single metal nanoparticle (MNP) on a conductive carbon support for testing as an electrocatalyst are described. Various approaches were investigated including interparticle distance enhancement, electrochemical and mechanical tip−substrate MNP transfer onto macroscopic surfaces, scanning electrochemical microscopy (SECM)-controlled electrodeposition, and the use of selective binding monolayers on carbon fiber electrodes (CFEs) for solution-phase-selective adsorption. A novel SECM technique for electrodepositing MNPs on CFE tips immersed 100−200 nm below the electrolyte level was developed and used to generate single Pt and Ni nanoparticles. Following their generation, we demonstrate electrocatalytic detection of Fe^{3+} on individual Pt particles with the CFE in a Fe^{3+}/H_2SO_4 solution. We also describe an approach of attaching MNPs to CFEs by controlling the composition of monolayers bonded to the CFE. By employing a monolayer with a low ratio of binding (e.g., 4-aminopyridine) to nonbinding molecules (e.g., aniline) and controlling the position of the CFE in a colloidal Pt solution with a SECM, we attached a single 15 nm radius Pt nanoparticle to the CFE. Such chemisorbed Pt particles exhibited a stronger adhesion on surface-modified CFEs and better mechanical stability during proton reduction than MNPs electrodeposited directly on the CFE.

Introduction

In recent years, metal nanoparticles (MNPs), especially Ag and Au, have been of interest because of their unique optical,[1,2] electrical,[3,4] magnetic,[5,6] and chemical[7−12] properties, often remarkably different from their bulk counterparts.[13−15] From a commercial standpoint noble MNPs, typically supported on high surface area carbons, are used in many heterogeneous catalytic and electrocatalytic processes.[16−24]

Of special interest is the relationship between the particle size and the structure with the chemical or electrochemical reactivity.[25−34] Several techniques have been used to investigate MNPs and nanostructured surfaces, including electrochemical methods,[35−39] IR spectroscopy,[40−42] X-ray absorption spectroscopy,[43,44] scanning tunneling (STM) and atomic force (AFM) microscopies,[45−47] differential electrochemical mass spectrometry (DEMS),[48] ultrahigh vacuum (UHV) techniques, and others.[49,50] Almost all studies of MNPs have involved large arrays or collections of particles on surfaces or dispersed in solution. These MNPs are typically prepared by bulk methods, e.g., collection of metal colloid particles from suspension by controlled adsorption[51−53] or electrophoresis,[54] vapor deposition of metal at low coverage onto a surface in high vacuum,[55] gas-phase reduction of metal salt particles by H_2,[56] microwave irradiation,[57] or electroless or pulsed potentiostatic deposition.[58,59] Significant problems that are typically encountered arise from difficulties in preparing MNPs with a narrow size distribution, surface agglomeration, occurrence of lattice defects, and poisoning of the metal by impurities (e.g., sulfur) present in the substrate support.[60,61]

Shifting from traditional multiple nanoparticle synthesis to synthesis and study of single nanoparticles can minimize these problems. While there have been extensive studies of single molecules, including catalytic properties of single enzymes, usually via fluorescence methods,[62] the behavior of single MNPs as catalysts remain relatively unexplored. In single molecule studies, the high signal amplification required is provided by the repeated excitation and emission of a suitable stable fluorescent label or product.[63] Amplification in electrocatalysis studies on single MNPs occurs by the repeated electron-transfer reactions that occur at the particle but require the detection of currents in the picoampere or sub-picoampere region. Moreover, a large variety of electrocatalytic reactions using solution phase reactants can be studied at a single MNP.

This paper deals with electrochemical methods of preparing and characterizing single MNPs. While single MNPs are more difficult to prepare compared to multiparticle collections, they provide several advantages, which are mainly related to reduced structural complexity. Unlike multiparticle-covered surfaces, single supported MNPs show no size or shape distributions and allow complex variables such as interparticle distance or particle surface density to be omitted from the analysis. From an electrochemical standpoint, the diffusion associated with multiple nanoparticles can be spherical, planar, or a combination of these, depending on the extent of overlap between the diffusion fields, which is governed by the spatial distribution of the particles on the support and is affected by several factors, such as the duration of the experiment. The equation for a diffusion-controlled reaction at a single nanoparticle is simpler showing, to a good approximation, spherical (or hemispherical) diffusion in accord with

$$J_{\lim} = nFDC_{\infty}/a \quad (1)$$

† Part of the special issue "Arthur J. Nozik Festschrift".

* Author to whom correspondence should be addressed. E-mail: ajbard@mail.utexas.edu.

10.1021/jp064434d CCC: $33.50
Published on Web 10/28/2006

where J_{lim} is the diffusion-limiting current density, n is the number of electrons transferred, F is Faraday's constant, D is the mediator diffusion coefficient, C_∞ is the mediator concentration, and a is the nanoparticle radius.

The equation demonstrates that diffusion current densities vary as a^{-1}, and hence for smaller particles it is possible to study fast interfacial reactions over a broad potential range, since the limit of diffusion is not reached even at considerable overpotentials. In synthesizing a nanoparticle for electrocatalytic studies, one seeks a number of desirable characteristics: (i) well-defined and known location of the nanoparticle; (ii) minimal electrochemical interference from the substrate; (iii) good adhesion to the substrate (high mechanical stability); (iv) controlled particle size and shape; (v) good contact (efficient bidirectional electron transfer) to the substrate; (vi) good chemical stability.

Despite these significant advantages, only a few reports have appeared on the electrochemistry of single MNPs.[64−68] Stimming and co-workers used an in situ method to prepare and measure the reactivity of single Pd nanoparticles on a Au support, reporting a strong size-dependent catalytic effect toward the proton reduction reaction.[64−66] In this study, particle preparation involved a modification of a method originally developed by Kolb et al. taking advantage of a fast response scanning tunneling microscope to place a single nanoparticle on a monocrystalline gold support.[69] Here we seek alternative, simpler techniques for both the generation and the electrochemical detection of single nanoparticles on electronically conductive substrates.

Experimental Section

Materials and Syntheses. All chemicals used were reagent grade and used as received. All aqueous solutions were prepared with deionized water (Milli-Q, Millipore Corp.). Dichloromethane (DCM, <0.001% H_2O) was obtained from Aldrich; dimethylformamide (DMF, 0.0037% H_2O) was obtained from Merck. Highly ordered pyrolytic graphite (HOPG, grade-1) was obtained from SPI Supplies (West Chester, PA); Carbon yarn (10 μm in diameter) was obtained from Strem Chemicals (Newburyport, MA). Anodic electrophoretic paint (Glassophor ZQ 84-43225) was from BASF (Münster, Germany) and diluted 1:20 with water prior to use. Silver epoxy was from Epoxy Technology (Billerica, MA).

cis-$PtPy_2Cl_2$ was synthesized by the method of Kauffman.[70] Au nanoparticle suspensions were prepared by a sodium citrate reduction of $HAuCl_4$ according to a method reported by Frens,[71] and the Pt nanoparticle suspension was prepared by hydrogen reduction of K_2PtCl_4 in the presence of the sodium salt of poly(acrylic acid), according to a method reported by Ahmadi et al.[72] The condensation reactions between oxidized CFEs and functionalized molecules followed a procedure by Xiolin et al., who used a similar methodology to immobilize single-walled carbon nanotubes on a gold substrate.[73]

CFE Tips. Glass pipets were prepared from borosilicate glass tubes (o.d. 1.2 mm, i.d. 0.69 mm) using a laser pipet puller (model P-2000, Sutter Instrument Co., Novato, CA), yielding micropipet tips with inner diameters of approximately 20 μm and tapers that were approximately 0.5 cm in length. Approximately 1 cm of the CFE that was 10 μm in diameter was attached to one end of a piece of Ni−Cr (Nichrome) wire using a small amount of silver epoxy and cured in an oven for 45 min at 100 °C. The wire/CFE assembly was then inserted into the top of the pulled micropipet and pushed through so that approximately 3 mm of the CFE protruded from the micropipet tip. Epoxy cement was injected into the top of the capillary to attach the Ni−Cr wire to the glass tube and hold the CFE rigid. The glass at the tip was then sealed around the CFE using a cool low oxygen/natural gas flame by inserting the pipet tip into the flame for approximately 0.5 s. The part of the CFE that protruded from the glass pipet was then flame etched in an oxygen-rich (bright blue) flame to a length of 50 μm or less using periodic observation by optical microscopy to monitor the progress of etching. During this step, it was very important to etch the CFE alone, without melting the glass seal. This was done by a very slow manual insertion of the CFE into the flame. An orange glow from the CFE indicated that etching was proceeding. Typically, three flame etches were performed, each lasting approximately 1 s. The etched carbon fiber was insulated with anodic electrophoretic paint. The etched CFE was immersed into a 1:20 solution of the paint in water, and a Pt coil surrounding the CFE was the reference/auxiliary electrode. A direct current potential of 2.2 V was applied to the CFE for 40 s, after which time the oxidation current had decreased to a small steady value of 0.2−1.0 nA. The electrode assembly was removed and heated at 150 °C for 3 min. This process has been shown to slightly shrink the deposited paint film, exposing the tip. The entire deposition and heating process was repeated once more to ensure good insulation of the sides of the fibers.

Instrumentation. A CH Instruments model CHI 900B (CH Instruments, Austin, TX) was employed for electrochemical measurements. Scanning electron microscopy (SEM) and energy-dispersive spectrometry (EDS) analyses were carried out using a LEO 1530 scanning electron microscope. Because the MNP was frequently smaller than the tip apex and sometimes located away from the apex, the CFEs were systematically SEM-imaged in a horizontal position and then flipped over and probed from the other side to cover the whole surface area.

Results and Discussion

Methods Involving Macroscopic Substrates. *Bulk Deposition.* MNPs can be prepared by direct synthesis on an inert macroscopic substrate, which can then be probed directly as a composite electrode, e.g., by scanning with a tip.[74] Figure 1 illustrates several approaches for generating single nanoparticles on larger (approximately millimeter) supports; this includes (A) controlled electrodeposition of MNPs with a low surface density, (B) on-contact mechanical transfer of a pre-deposited MNP on a tip, and (C) MNP formation on substrate by electrochemical oxidation at a tip.

The electrochemical generation of MNPs occurs through a nucleation and growth mechanism.[75] The process starts by reduction and adsorption of solution phase cations at defect sites of the substrate (e.g., edge planes on HOPG). In the next stage, surface diffusion of the adatoms leads to competing processes of aggregation and desorption, which primarily depend on the adsorption energy and interactions with the substrate. During aggregation, incorporating an increasing number of adatoms forms stable nucleation centers, and three-dimensional particle growth begins. On macroscopic substrates, a large number of nucleation centers coexist due to many intrinsic surface defects. Under such circumstances, generation of a single MNP is highly improbable. However, when the surface density of the particles is decreased, it is possible to separate the MNPs to a sufficient distance that the spherical diffusion fields of individual particles will not overlap (Figure 1A). At that stage single MNPs can be examined by a scanning probe method. (For example, a carbon nanofiber can be used to approach small entities by the scanning electrochemical microscopy (SECM) collection/generation mode, allowing their study at a short distance).

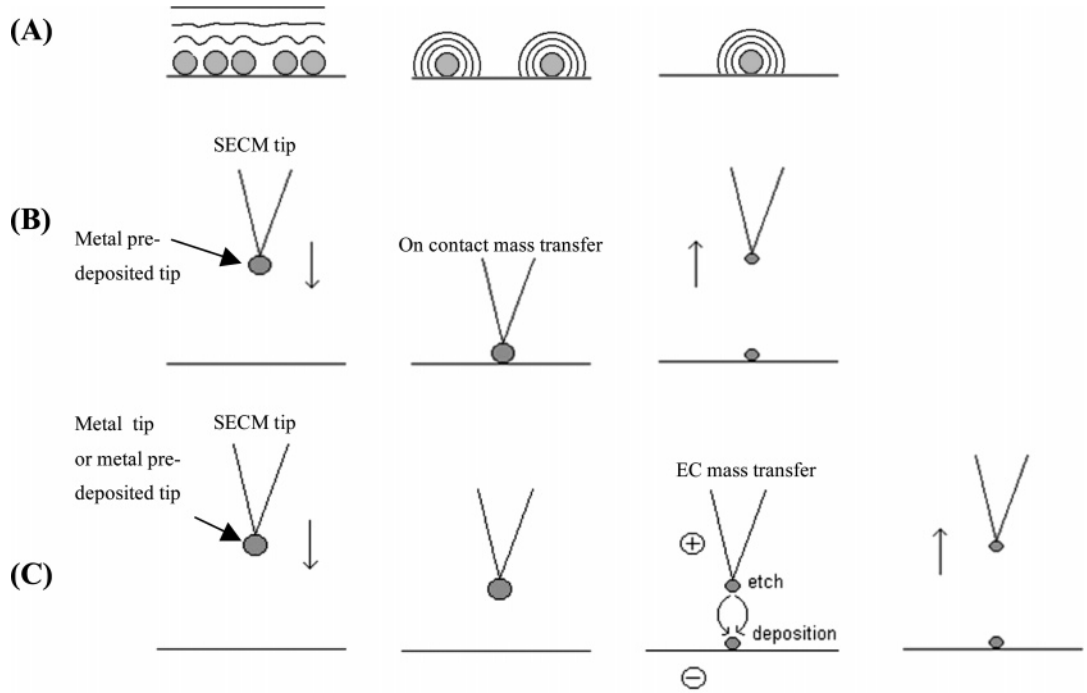

Figure 1. Schematic presentation of different techniques employed to fabricate single or well-spaced individual nanoparticles on a macroscopic area HOPG, with or without microtips: (A) decreasing nanoparticle surface density by controlled electrodeposition; (B) on-contact mechanical particle transfer between tip/substrate; (C) electrochemical mass transfer between tip/substrate.

We have tested several approaches for MNP surface density dilution, including: (i) minimizing surface defects on the substrate (i.e., by using a freshly cleaved HOPG of the highest available grade); (ii) decreasing the electrolyte concentration; (iii) working in a diffusion-controlled overpotential region, which increases the effect of the nucleation exclusion zones around the growing nucleation centers.[77] Our observations indicate that a significant decrease in Pt nanoparticle surface density was indeed evident using these guidelines, but in all cases and even when shorter deposition pulses were applied, the surface distribution of the generated particles still produced a very short interparticle distance. The transition from spherical to planar total diffusion happens within a very short time, given by

$$t_d \cong R'^2/2D \qquad (2)$$

where t_d is the time for transition from spherical to planar diffusion, R' is the half distance between closest neighboring nanoparticles, and D is the diffusion coefficient of the mediator species.

Unfortunately, during the measurements we consistently observed small interparticle distances. Figure 2A shows a SEM image of Pt NPs on HOPG, electrodeposited from a 0.1 mM H_2PtCl_4, 0.1 M H_2SO_4 solution with a 100 ms pulse to $E = -600$ mV vs Hg/Hg_2SO_4. Although individual MNPs can be discerned, R' values on the order of a few tens of nanometers were obtained. The deposition current, $i(t)$, which accompanied the measurement, fit a $t^{-1/2}$ behavior in accord with planar (Cottrell) diffusion. The transition from spherical to planar diffusion occurred within a few milliseconds, too short an experimental time to easily probe a single MNP with no interference from neighboring particles. (Locating a probe tip significantly closer to a single MNP than its neighbors is technically challenging.[76])

In an effort to further increase the interparticle distance, Pt electrodeposition on HOPG from organic solvents was attempted. Under similar conditions, reduction of $PtPy_2Cl_2$, dissolved in 0.1 M tetrahexylammonium fluoroborate ($THABF_4$) in DCM exhibited an order of magnitude smaller deposition currents compared to the aqueous solutions (Figure 3), apparently because of lower electrolyte conductivity, a smaller Pt(II) diffusion coefficient, and different solvent/graphite/particle

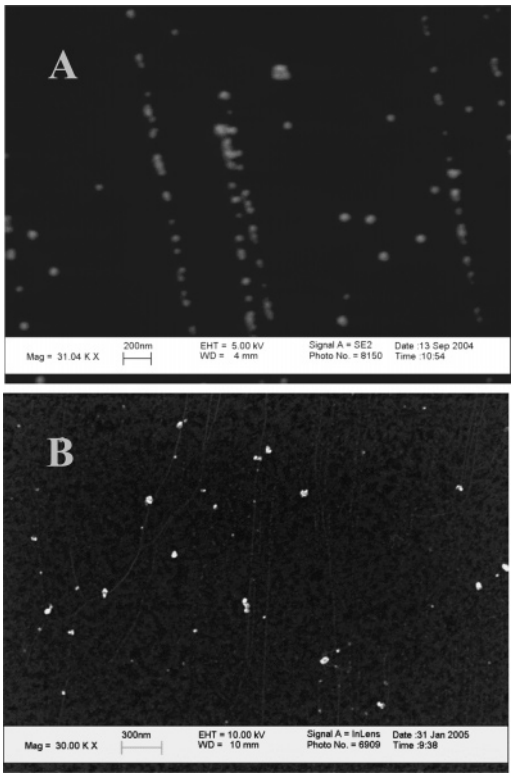

Figure 2. SEM images of HOPG following potentiostatic electrodeposition for 100 ms at −600 mV vs Hg/Hg_2SO_4 from: (A) 0.1 mM H_2PtCl_6 in 0.1 M H_2SO_4; (B) 0.1 mM $PtPy_2Cl_2$ and 0.1 M $THABF_4$ in DCM.

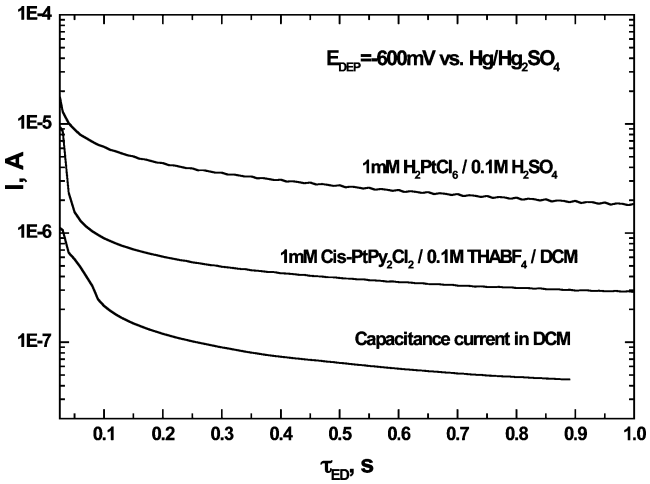

Figure 3. Potentiostatic ($E = -600$ mV vs Hg/Hg_2SO_4) electrodeposition of Pt on HOPG from aqueous and organic Pt solutions. The capacitance current was measured in 0.1 M $THABF_4$/DCM. The electrolyte was introduced and removed from the cell with the electrode biased at $E = 0$ mV vs Hg/Hg_2SO_4 before and after contact with electrolyte to prevent spontaneous electroless Pt deposition. A large surface Pt coil was the counter electrode mounted above the HOPG.

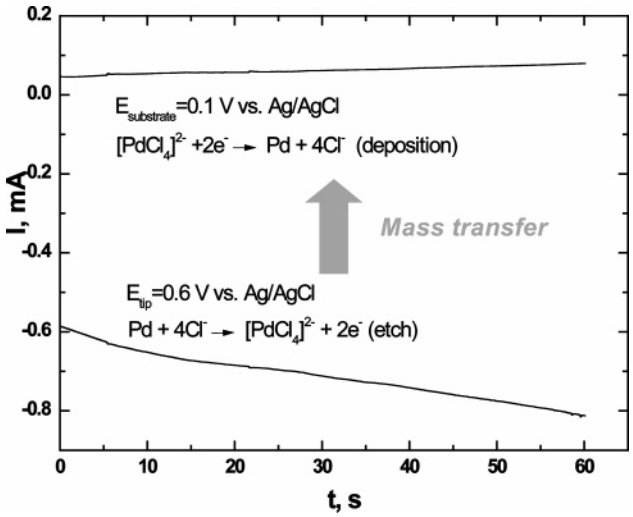

Figure 4. Electrochemical mass transfer from a Pd conical UME (radius at apex 1 μm) to a HOPG substrate subject to a 60 s pulse. $E_{tip} = 0.6$ V; $E_{substrate} = 0.1$ V vs Ag/AgCl. Electrode gap, ~200 μm. Electrolyte, 4:16:80 $HCl_{(conc)}/CaCl_{2(sat)}/H_2O$ (v/v).

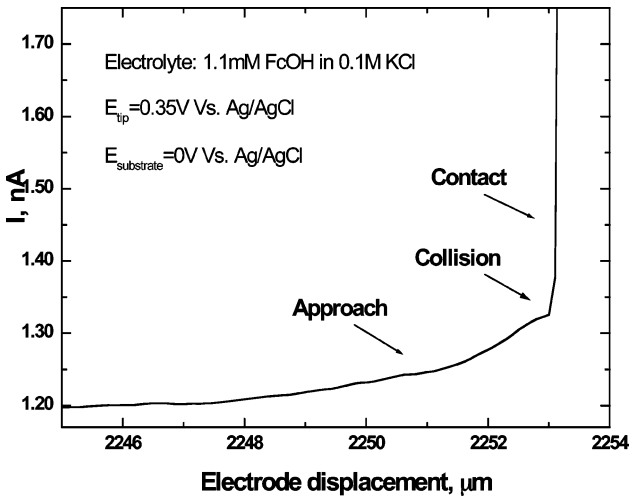

Figure 5. Approach curve to a point of contact between Pd-coated conical carbon tip (radius at apex, ~2 μm) and HOPG substrate in 1 mM FcMeOH/0.1 M KCl. Approach rate, 1 μm s^{-1}.

interactions that affect the surface tension and growth of the particles. Despite the marginal increase in the estimated interparticle distance to 100−200 nm, which is evident in Figure 2B, significant diffusion layer overlap still occurred for periods longer than the millisecond range. We conclude that neither aqueous nor organic phase electrodeposition on macroscopic substrates are effective for the generation of separated MNPs needed for a simple electrochemical ex situ detection.

Anodization of Tip Material. A different method involves local deposition by anodization of an ultramicroelectrode (UME) tip (Figure 1C) and deposition of a MNP on the substrate (electrochemical patterning).[78] In this method a carbon fiber preloaded with a small amount of a metal or alternatively a sharp conical tip of the desired metal is brought near a HOPG substrate, e.g., using the feedback mode of the SECM with a suitable redox mediator (e.g., ferrocene methanol (FcMeOH)). A suitable etching solution of $CaCl_{2(sat)}/H_2O/HCl_{(conc)}$ (e.g., for Pt 60:36:4 (w/w)) is then added to the cell, and both the substrate and the tip are concurrently polarized. The tip is held at a positive potential where it is anodically etched, and the metal cations migrate to the surface of the substrate where the potential is sufficiently negative for electrodeposition. Clearly, this method is favorable for metals where electrochemical etching is facile. Figure 4 shows chronoamperometric responses to a 60 s potential pulse simultaneously applied to a Pd metal conical tip (0.6 V) and a HOPG substrate (0.1 V). The increase of both the etching and the deposition currents with time results from increasing exposure of the tip surface and the subsequent gradual increase in the flux of cations migrating to the substrate. A combined SEM/EDS analysis of the substrate following these experiments confirmed the formation of Pd nanoparticles by tip−substrate electrochemical mass transfer, densely distributed around the tip position during pulsing. A possible solution for this multi-MNP deposition may be to minimize the electrode gap or to use smaller tips. This requires close control of the tips over nanometer gaps. Although this is possible,[76] it frequently leads to tip−substrate crashes and significant damage.

Mechanical Transfer of the Nanoparticle from the Tip. Tip and substrate crashes can be used for mechanical (rather than electrochemical) particle transfer (Figure 1B). Here, a sharp carbon microtip with an electrodeposited Pd NP was vertically directed toward the surface of a HOPG substrate, while both electrodes were immersed in FcMeOH electrolyte. An approach curve, shown in Figure 5, was taken with the tip potential set to oxidize the mediator and the substrate held at the potential for $FcMeOH^+$ reduction. When the tip reached the vicinity of the HOPG, the positive feedback current became significant and gradually increased. When the tip hit the surface of the graphite, as indicated by a steep increase in the current, a small fraction of the deposited Pd on the tip mechanically transferred to the substrate. A fast retraction of the tip was immediately performed upon detection of the contact current. In such experiments, we consistently observed damage to both the tip and the substrate. Cyclic voltammetry at the tip before and after the collision with the surface showed a significant increase of the FcMeOH steady-state limiting oxidation current with occasional transitions from an UME voltammogram to that typical of a macroscopic electrode. Furthermore, the damage to the electrodes could be observed optically or by SEM. Under such conditions detection of the transferred single nanoparticle on the HOPG was impossible to achieve. Efficient mechanical MNP transfer was observed with fast response STM,[64−66,69] considering also the enhanced sensitivity of STM at nanometric tip/substrate gaps

compared to that of SECM. Nevertheless, STM is not easily compatible with subsequent electrochemical measurements.

In our hands all of the methods discussed so far suffered from various problems and hence seem less effective to the generation of single MNPs as electrocatalysts. The use of a probing tip to characterize the nanoparticle is challenging, and a reliable analysis requires a bare, untreated tip. For this reason we examined alternative techniques to generate and electrochemically detect a single MNP.

SECM Mediator Positioning Technique. As opposed to macroscopic substrates, single nanoparticle formation on microscopic substrates such as the apex of a sharpened carbon fiber offers several advantages. First, localization of the nanoparticle within a very limited area prevents the need to track it down over a large substrate surface. Moreover, from an electrochemical point of view, small UMEs support smaller double-layer charging currents and shorter RC time constants that significantly increase the sensitivity of detection.[79]

Carbon fiber electrodes provide several additional advantages: (1) They can be easily flame etched to obtain a radius of curvature of 50−250 nm; (2) after insulation, the CFE apex shows a low (<0.5) aspect ratio that is useful in SECM experiments since higher sensitivity to feedback current increases with flat, disklike geometry;[76] (3) carbon electrodes show high intrinsic overpotentials for proton and oxygen reduction so that CFEs can be used to electrodeposit MNPs from acidic media and to study electrocatalytic effects of the nanoparticles with respect to these reactions.

However, the biggest difficulty with a CFE tip is forming a pinhole-free insulation layer with a well-defined exposed end. Although we have occasionally observed tips with nearly perfect insulation by coating with anodic electrophoretic paint (with an electrochemically evaluated area approaching 160 nm^2), reproducing the same coating procedure of the CFE results in the formation of a thin polymer-insulating layer with a random distribution of tiny pinholes. The occurrence of such pinholes is clearly evident in the SEM images of Figure 6 where electrodeposition was performed on a fully immersed, electrophoretically insulated CFE in Pt and Pd solutions. In the absence of electrodeposition control, MNPs grow at the pinholes (Figure 6A), and when the deposition charge is significantly increased, surface aggregation leads to gradual coverage of the carbon by metal (Figure 6B). These pinhole effects must be minimized during the generation of the single nanoparticles, so a different approach based on slow electrode displacement controlled by SECM and sensitive detection of mediator redox currents at the air/electrolyte with SECM was used.[80,81] This method is illustrated in Figure 7, with experimental results in Figure 8. A CFE tip is held in air above a composite electrolyte containing (1) cations of the metal (M) to be electrodeposited, (2) a redox mediator, and (3) the supporting electrolyte. The tip is first held at a potential where the mediator exhibits considerable redox current at potentials where electrodeposition does not occur, i.e., E_{tip} (mediator redox) > E_{DEP} ($M^{n+} + ne^- \rightarrow M$).

With the right combination of metal cation and mediator the tip contacts the solution at a potential where electrodeposition does not occur.[58] The tip is slowly directed toward the surface of the electrolyte using piezoelectric control, where the tip in air displays only the SECM potentiostat offset current (~800 fA). Upon just touching the liquid surface, a current spike combined from mediator redox Faradaic and double-layer charging currents appears and quickly decays to a Faradaic steady state. The tip is then stopped at 100−150 nm below the solution level, exposing its small apex to the electrolyte. If the tip is not deliberately halted at this stage, then an extended curve in liquid is collected, which sometimes shows multiple current spikes associated with pinholes in the CFE. At this stage, after positioning via the mediator responses, a short (500 ms) electrodeposition potentiostatic pulse is applied to the CFE. A response to such a pulse (Figure 8, inset) shows a typical increase in the deposition current, proportional to the square root of the deposition time, indicating the growth of a single nucleation center (discussed later). Unlike electrodeposition on macroscopic HOPG, there is no overlap between the diffusion fields of neighboring nucleation centers on the CFE, and the overall diffusion is spherical.

Two difficulties in this electrochemical tip positioning method arise from electrolyte evaporation and the formation of a

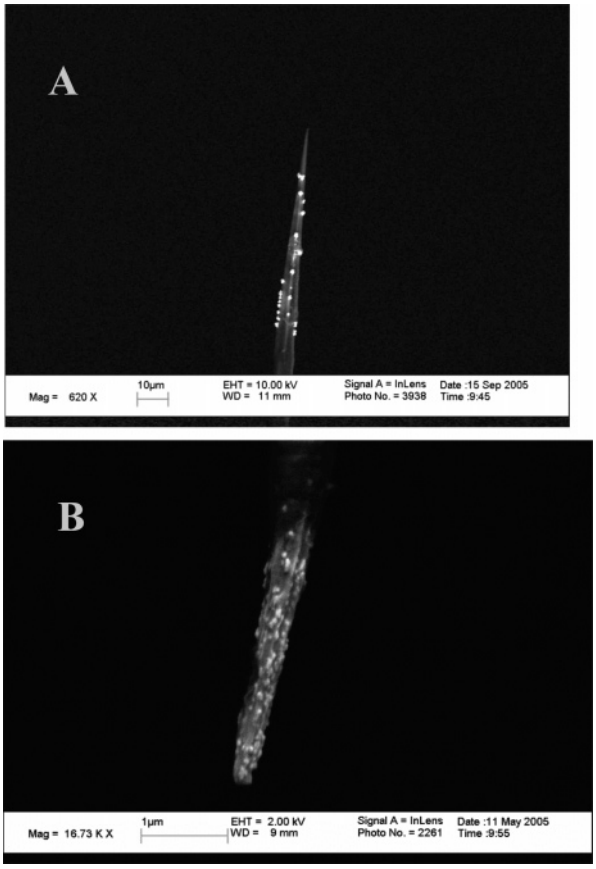

Figure 6. Electrodeposition on CFE tips at full immersion. (A) Pt from 1 mM K_2PtCl_6/0.1 M HCl for 10 s at −150 mV vs Ag/AgCl; (B) Pd from 0.75 mM $PdCl_2$/5 mM $HClO_4$/50 mM $NaClO_4$ by sweeping the potential linearly five times from 0.6 to 0.0 V vs Ag/AgCl at 50 mV s^{-1}.

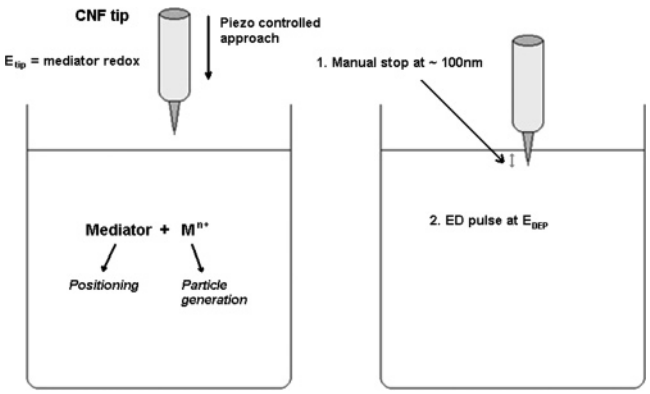

Figure 7. Schematic of the SECM mediator positioning technique.

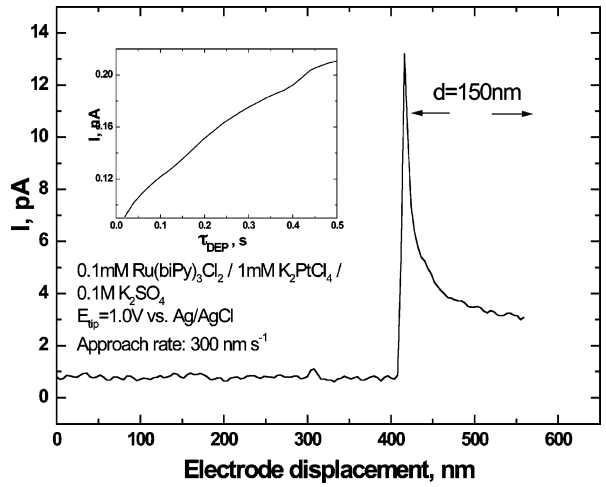

Figure 8. CFE approach from air to an electrolyte containing $Ru(bpy)_3Cl_2$ mediator and Pt(II) at $E_{tip} = 1.0$ V vs Ag/AgCl. The approach was stopped at a depth of 150 nm, and a potentiostatic deposition pulse was applied. The chronoamperometric response to a pulse at $E_{DEP} = -0.5$ V vs Ag/AgCl is shown in the figure inset.

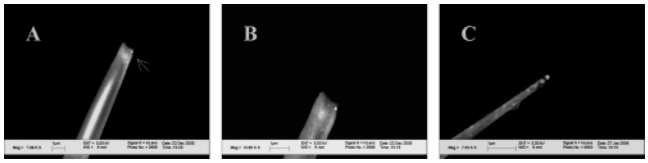

Figure 9. SEM images of two single Ni nanoparticles obtained from 1 mM $NiCl_2$/0.85 mM FcMeOH/0.1 M KCl solution. For all cases, $\tau_{DEP} = 100$ ms and $E_{DEP} = -1.05$ V vs Ag/AgCl. Figures 9A and 9B are different magnifications of a single particle located ~150 nm from the CFE edge. Figure 9C presents a single particle deposited directly at the CFE apex.

meniscus between the tip and the liquid phase (schematically presented in Figure S3 of the Supporting Information). The first interference is overcome by fixing the approach rate above the evaporation rate. This was measured by successive tip approaches at different rates, which detect the incremental change in the level of solution with time, and was observed to be $V_{vap} \approx 22-28$ nL s^{-1}, equivalent in our 8 mm radius cell to 0.10−0.14 μm s^{-1} *z*-movement of the tip, at $T = 20$ °C and $P = 1$ atm. Meniscus problems became less pronounced when the tip was immersed less than 400 nm into the solution. SEM images taken for tips electrodeposited at deeper immersion often detected nanoparticles at heights exceeding 1 μm from the apex of the CFE.

The mediator positioning technique was employed in the preparation of single Ni and Pt nanoparticles (with either 1 mM $NiCl_2$/1 mM FcMeOH/0.1 M KCl or 1 mM K_2PtCl_4/0.25 mM $Ru(bpy)_3Cl_2$/0.1 M K_2SO_4 solutions, respectively). Figure 9 shows two single Ni nanoparticles with radii of 60 ± 10 nm. A focused EDS analysis was used to confirm the metallic composition of these particles. While the particle in Figures 9A and 9B is located ~150 nm from the CFE edge, that in Figure 9C is at the CFE apex. Pt nanoparticles with similar, ~60 nm, radii were similarly obtained by applying 500 ms deposition pulses at $E_{DEP} = -0.50$ V vs Ag/AgCl. Upon deposition at deeper immersion (>400 nm) a significant meniscus was formed, and the Pt nanoparticles showed a clear tendency to align in straight lines along the CFE main axis (also shown in Figure 6A), a phenomenon previously observed in the electrodeposition of Pt NPs on HOPG,[58] where the particles favor growing on step edges in the graphite basal plane. Possibly, by analogy to the existence of step edges on the surface of HOPG, sharp carbon edges are formed during the etching of the fiber in the flame. These constrain the surface diffusion of the Pt adatoms during nucleation and hence localize the nucleation centers in their vicinity, leading to favored nanoparticle growth at pinholes located along the carbon edges.

Electrochemical Detection of a Single Nanoparticle. Electrochemical detection of single MNPs on conductive substrates is challenging and requires several conditions to be met. One must distinguish electrochemically the nanoparticle from its surrounding support material from known electrochemical behavior (Figure S1 of the Supporting Information) and be able to detect the small redox currents associated with the tiny particle. Moreover, we must ensure that the electrochemical reaction and its products will not change the nanoparticle and leave it intact. A benefit of Pt NPs is chemical stability and electrocatalytic effects in several reactions. Electrochemical detection of Pt can be carried out using selective mediators, which are catalytically active on Pt and at the same time show sluggish kinetics on carbon, e.g., H^+ and O_2 reduction reactions. Figure S1 of the Supporting Information shows an overpotential difference of more than 0.4 V between Pt and C toward proton reduction reaction as well as irreversible and hindered kinetics on the carbon. In addition, other distinctive features of Pt are typically observed during cycling in strongly acidic solutions. These fingerprints include characteristic hydrogen adsorption/desorption waves, Pt oxide formation, and its corresponding reduction peak. Assuming that the nanoparticle possesses a hemispherical shape, eq 1 can be simplified and used to calculate the expected diffusion-limited currents for reduction of 10 mM H^+ (5 mM H_2SO_4), according to

$$i_{lim} = 2\pi nFDC_{\infty}a \qquad (3)$$

In accord with eq 3 and by disregarding possible size-dependent catalytic effects for smaller-size particles, the expected diffusion-limiting currents for 1−100 nm Pt nanoparticles in 10 mM H^+ are on the order of 0.1−10 nA, which are readily measured. The currents associated with the waves of hydrogen adsorption and desorption on the Pt surface are much smaller. Considering an adsorption of a full monolayer of H atoms on a $a = 70$ nm polycrystalline Pt nanoparticle taking $Q_H = 210$ μC cm^{-2} for cyclic voltammetry at 1 V s^{-1}, the average current expected for the hydrogen waves is on the order of sub-picoampere, which makes detection by this route very difficult. The same problem occurs with underpotential deposition (UPD) of metals such as Cu, Pb, Sn, Ag, Tl, and Bi, which all support monolayer charge densities below 400 μC cm^{-2} on Pt and hence do not significantly increase the detection currents.

While performing cyclic voltammetry for CFEs deposited with Pt single nanoparticles in 0.5 M H_2SO_4, we observed a rapid detachment of the particle from the CFE surface at the onset of proton reduction. This suggests that the individual MNPs are held on carbon by weak physisorption[58] not evident in cases of larger metallic clusters such as those in Figure 6. The use of O_2 reduction for detection, which eliminates gas evolution, although possible,[82] is limited by the low oxygen solubility (<2 mM) in water at 25 °C, which decreases the detection current because of a smaller concentration term in eq 3.

A good mediator, which supports preferential, enhanced kinetics on Pt compared to carbon and no generation of a disrupting gas is the Fe^{3+}/Fe^{2+} couple.[83,84] At pH 0, both species of the iron are moderately soluble and do not cause any mechanical or passivation hazards to the nanoparticle. At ~5 mM in 1 M H_2SO_4, Fe^{3+} was first used to detect Pt NPs

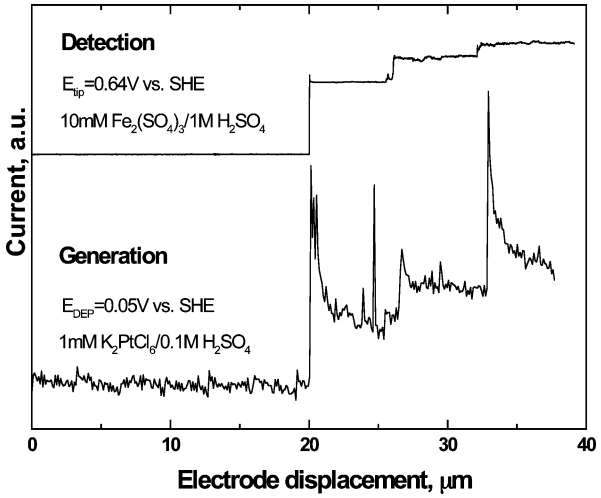

Figure 10. Lower curve: Generation of Pt nanoparticles on a CFE tip moving from air to a Pt(II) solution under active electrodeposition tip potential. Upper curve: Detection of the Pt nanoparticles on the tip by approach from air to a Fe^{3+}/H_2SO_4 solution at a potential supporting electrocatalytic Fe^{3+} reduction on Pt.

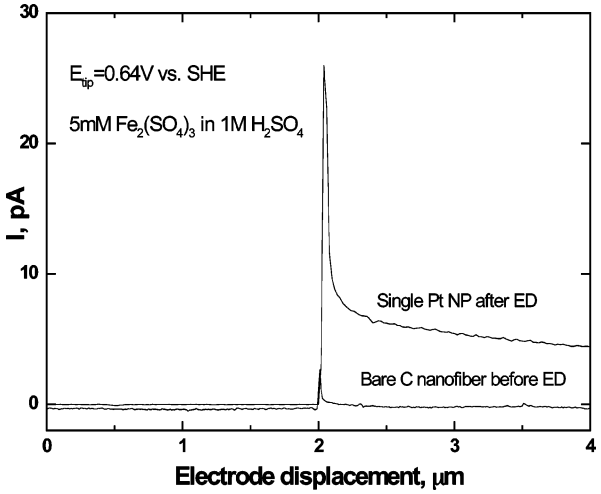

Figure 11. Approach from air curves for a CFE tip moving from air to Fe^{3+}/H_2SO_4 before and after the deposition of a single Pt nanoparticle according to the mediator positioning technique (deposition from 1 mM K_2PtCl_4/0.25 mM $Ru(bpy)_3Cl_2$/0.1 M K_2SO_4 solution for 0.5 s at E_{DEP} = −0.50 V vs Ag/AgCl).

electrodeposited along an insulated CFE (Figure 10). In the beginning of this experiment the CFE was held at the deposition potential of Pt, and an air approach measurement was performed, allowing the tip to travel more than 18 μm below the solution level. The current spikes observed in the figure along with the tip displacement correspond to the generation of Pt deposition centers through occasional pinholes. The current decay that follows the spikes suggests an overlapping of close particle diffusion fields. At the end of the generation stage, the tip was backed out, the solution was replaced by $Fe_2(SO_4)_3$ in 1 M H_2SO_4, and a second approach from air was performed, with the tip potential at E_{tip} = 0.64 V vs the standard hydrogen electrode (SHE). As can be seen in the upper portion of Figure S1 in the Supporting Information, this potential allows one to distinguish between the Pt nanoparticle and the carbon substrate, since it solely supports the electrocatalytic reduction of Fe^{3+} to Fe^{2+} on Pt. Figure 10 demonstrates a good correlation between the generation and the detection peaks along the CFE from which it is clear that the Fe^{3+} mediator provides good selectivity in tracking the deposited Pt particles on the composite substrate.

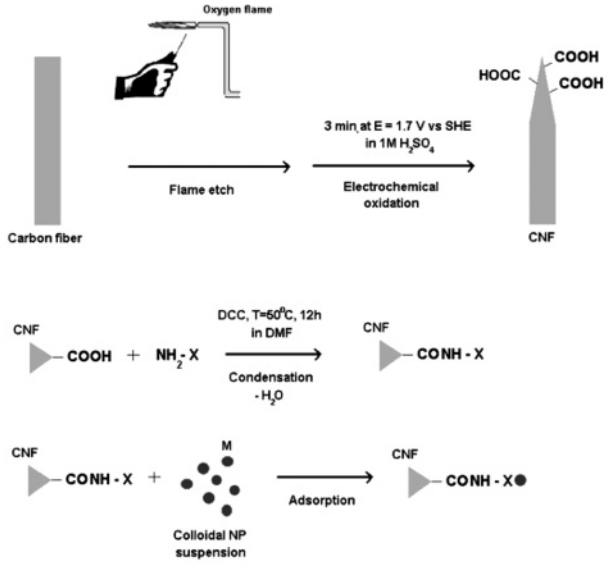

X = 4-aminothiophenol (M=Au)

X = 4-aminopyridine (M=Pt)

Figure 12. Schematic of the binding monolayer approach for adsorbing Au and Pt MNPs from colloidal solutions on modified CFE tips and controlling their surface concentration.

SEM analysis indicated a good geometrical agreement with those observations.

Although detection of ensembles of NPs was demonstrated, detection of a single Pt nanoparticle is more difficult. Figure 11 shows two air approach measurements in Fe^{3+}/H_2SO_4 performed on the same CFE before and after the growth of a single Pt nanoparticle using the mediator positioning technique (under similar conditions to those presented in Figure 8). As can be seen, in the presence of the single particle, a 20-fold increase in the steady-state current was evident. To evaluate the correlation between the detection current and the real dimensions of the particle, we first estimated the radius associated with the electrochemical generation. This can be done by equating the hemispherical diffusion current in eq 3 to the spatial growth rule provided by Faraday's law

$$2\pi nFDC_\infty a = (nFd_{Pt}/M_{Pt})(dV_{Pt}/dt) = nFd_{Pt}2\pi a^2(da/dt)/M_{Pt} \quad (4)$$

where V_{Pt} is the volume of the Pt nanoparticle, d_{Pt} is the density of Pt, and M_{Pt} is the molar mass of Pt.

Hence, under potential supporting diffusion-limited current, the time-dependent deposition current conditions and nanoparticle radius are, respectively

$$i(t) = n\pi F((2DC_\infty)^3 M_{Pt} t/d_{Pt})^{1/2} \quad (5)$$

$$r(t) = (2DC_\infty M_{Pt} t/d_{Pt})^{1/2} \quad (6)$$

An electrodeposition pulse width of t = 0.5 s yields a radius of 70 nm, which is in good agreement with SEM observations. According to eq 3 with $D_{Fe(III)} = 1.2 \times 10^{-6}$ cm^2 s^{-1},[85] a detection current corresponding to this radius would be $i_{ss} \approx$ 25 pA.

Binding Monolayers and Particle-Adsorption Methods. The interaction between the electrodeposited NPs and the carbon support can be strengthened by the use of bifunctional molecular

binding layers. As shown in Figure 12, a CFE can chemically react and subsequently attach to a layer of binder (e.g., 4-aminothiophenol) with a high affinity toward MNPs (e.g., Au). The process of attaching the binder to the CFE requires it to have surface carboxylic groups, which are formed during the oxidation of the carbon fiber in the oxygen-enriched flame[86−88] or by electrochemical oxidation for 180 s at $E = 1.7$ V vs SHE in 1 M H_2SO_4. The oxidized CFEs were then heated for >12 h at 50 °C in DMF solutions containing 1 mM of 4-aminothiophenol (for binding Au nanoparticles) or 4-aminopyridine (for binding Pt nanoparticles). The organic amine molecules are relatively short and contain a conjugated aromatic ring to provide facile electron transfer between the MNP and the CFE. The condensation reaction is carried out in the presence of 1,3-dicyclohexylcarbodiimide (DCC), which facilitates dehydration and binding via amide bonds. The modified CFE tips were then immersed into a solution of colloidal Au or Pt nanoparticles, where strong adsorption forces attach them to the S (Au) or to the pyridine nitrogen (Pt) termini. Shown in Figure S2 of the Supporting Information CFE tips in the absence (A) or in the presence (C) of 4-aminopyridine surface modification following immersion for 15 min in a unstirred Pt nanoparticle (∼30 nm diameter) suspension and rinsing in water. As demonstrated, the presence of a molecular binding layer is essential for the linkage of the Pt nanoparticles to the CFE, and in such cases a high surface density with an estimated nanoparticle radius of $a \approx 15$ nm is evident.

However, to reduce the surface density of the NPs, desirably to the single MNP level, one must dilute the binder by similar molecules that do not bind to the metal, i.e., "blocking" molecules such as aniline (Figure S3 of the Supporting Information). The dilution effect is evident in Figure S2B of the Supporting Information for a CFE incubated for 16 h in the presence of 1:200 4-aminopyridine/aniline solution in DMF, showing fewer Pt nanoparticles on the surface compared to part C. A further decrease in the surface density can be accomplished by decreasing the binder/blocker molar ratio, decreasing the concentration of DCC, and decreasing the temperature or shortening the condensation period. This can also be accomplished by careful control of the SECM tip positioning at the air/liquid (NP solution) interface. Here, the chemically modified apex of the CFE tip is immersed only a few hundred nanometers below the metal NP solution level (Figure S3 of the Supporting Information). The tip is held at this position for a short time (the time is delayed until electrolyte evaporation forces the apex outside the liquid, gradually leaving more contact time for the apex edge) in which the randomly moving MNPs can attach. Care must be taken not to oxidize the immobilized molecules, and hence the approach scan is made with the modified tip only slightly polarized with respect to a combined counter/reference electrode (0.02 V). Under such conditions the modified CFE approaches a mediator-free colloidal solution without generating Faradaic current but only a double-layer charging current that indicates the point of penetration. Upon a successful adsorption shown in Figure 13, we were able to obtain a single Pt nanoparticle bound to a pyridine on the CFE. As opposed to the case of the electrodeposited Pt single nanoparticle, repeated cyclic voltammetry performed in sulfuric acid showed a proton reduction wave at the onset of $E = 0.0$ V vs SHE, with no loss of the Pt NP (Figure S4 of the Supporting Information). Thus efficient electron transfer supporting minimal potential losses occurs between the particle and the CFE through the monolayer, probably because of the relatively short and conjugated structure of the 4-aminopyridine molecule. Enhanced cohesion forces are evident by chemisorption of the particle on the monolayer. This interaction between the pyridine nitrogen and the Pt metal[89] is significantly stronger than the net physisorption associated with a Pt particle generated by electrodeposition on carbon.

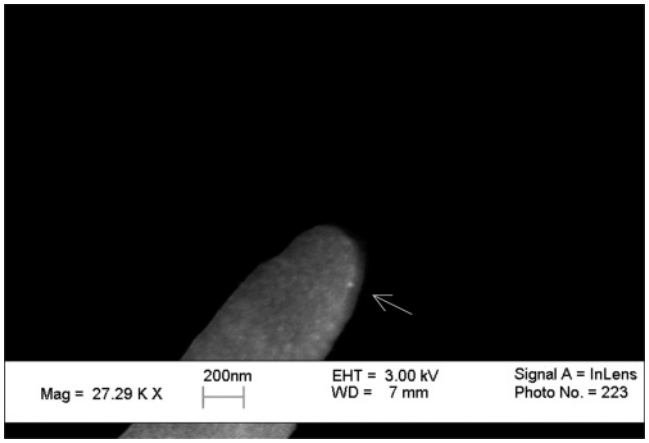

Figure 13. SEM image of a single Pt nanoparticle, chemisorbed on the surface of a CFE modified by 1 mM 4-aminopyridine and 200 mM aniline. The tip was immersed at 350 nm below the surface level of a Pt colloidal suspension using SECM air approach while monitoring the capacitance current at $E_{tip} = 0.02$ V vs Pt reference/counter electrode.

Conclusions

While methodologies such as particle separation by pulsed electrodeposition, electrochemical, and mechanical (SECM-assisted) material transfer from tip to a macroscopic carbon substrate show several problems that hinder the generation of remote or single nanoparticles, a combination of a carbon nanofiber tip and SECM piezoelectric-controlled positioning demonstrates a fast and novel solution. Generation of isolated $a = 60 \pm 10$ nm Pt and Ni particles is facile by short pulse electrodeposition on CFE tips, which are immersed, using controlled electrochemical positioning, about 100−200 nm below the surface level of a combined electroplating and mediator solution. An alternative method is to attach a binding monolayer to the CFEs via condensation of amine-terminated molecules and surface carboxylic acid groups. Strict control over the ratio of binding to blocking functionalities in the monolayer directly affects the surface density of Au and Pt nanoparticles adsorbed on the surface upon immersion in metal colloidal solutions. Combining the SECM-assisted positioning technique with this method allows the chemisorption of a single Pt nanoparticle onto the pyridine-terminated molecules, which demonstrates favored mechanical stability toward hydrogen evolution compared to that of the physisorbed electrodeposited particle. A further advantage of this method is that the particle size here is determined by the synthetic procedure of the suspension (that typically involves electroless reduction of the metal salt to a finely monodispersed colloid), which is significantly easier to control compared to both electrochemical generation and mechanical particle transfer.

Acknowledgment. This work was supported by a grant from the National Science Foundation (Grant No. CHE 0451494). R.T. thanks the Israel Science Foundation and the Technion−Israel Institute of Technology for a postdoctoral fellowship.

Supporting Information Available: Additional cyclic voltammetry and SEM figures. This material is available free of charge via the Internet at http://pubs.acs.org.

References and Notes

(1) Haes, A. J.; Van Duyne, R. P. *J. Am. Chem. Soc.* **2002**, *124*, 10596.
(2) Pivin, J. C.; Garcia, M. A.; Hofmeister, H.; Martucci, A.; Vassileva, M. S.; Nikolaeva, A.; Kaitasov, O.; Llopis, J. *Eur. Phys. J.* **2002**, *20*, 251.
(3) Graf, H.; Vancea, J.; Hoffmann, H. *Appl. Phys. Lett.* **2002**, *80*, 1264.
(4) Braun, M.; Link, S.; Burda, C.; El-Sayed, M. *Chem. Phys. Lett.* **2002**, *361*, 446.
(5) Shemer, G.; Markovich, G. *J. Phys. Chem. B* **2002**, *106*, 9195.
(6) Chen, D. H.; Hsieh, C. H. *J. Chem. Mater.* **2002**, *12*, 2412.
(7) Kamat, P. V. *J. Phys. Chem. B* **2002**, *106*, 7729.
(8) Liu, J.; Ong, W.; Kaifer, A. E.; Peinador, C. *Langmuir* **2002**, *18*, 5981.
(9) Rodriguez, J. A.; Liu, G.; Jirsak, T.; Hrbek, J.; Chang, Z. P.; Dvorak, J.; Maiti, A. *J. Am. Chem. Soc.* **2002**, *124*, 5242.
(10) Lou, Y. B.; Maye, M. M.; Han, L.; Luo, J.; Zhong, C. J. *Chem. Commun.* **2001**, 473.
(11) Yonezawa, T.; Imamura, K.: Kimizuka; N. *Langmuir* **2001**, *17*, 4701.
(12) Templeton, A. C.; Hostetler, M. J.; Kraft, C. T.; Murray, R. W. *J. Am. Chem. Soc.* **1998**, *120*, 1906.
(13) Feldheim, D. L.; Foss, C. A., Jr. *Metal Nanoparticles: Synthesis, Characterization, and Applications*; Marcel Dekker: New York, 2002.
(14) Trindade, T.; O'Brien, P.; Pickett, N. L. *Chem. Mater.* **2001**, *13*, 3843.
(15) Schmid, G. *Chem. Rev.* **1992**, *92*, 1709.
(16) Wang, J. X.; Markovic, N. M.; Adzic, R. R. *J. Phys. Chem. B* **2004**, *108*, 4127.
(17) Kabbabi, A.; Gloaguen, F.; Andolfato, F.; Durand, R. J. *Electroanal. Chem.* **1994**, *373*, 251.
(18) Freelink, T.; Visscher, W.; Van Veen, J. A. *J. Electroanal. Chem.* **1995**, *382*, 65.
(19) Yahikozawa, K.; Fujii, Y.; Matsuda, Y.; Nishimura, K.; Takasu, Y. *Electrochim. Acta* **1991**, *36*, 973.
(20) Watanabe, M.; Sei, H.; Stonehart, P. *J. Electroanal. Chem.* **1989**, *261*, 375.
(21) Kinoshita, K. *J. Electrochem. Soc.* **1990**, *137*, 845.
(22) Hirai, H.; Wakabayashi, H.; Komiyama, M. *Chem. Lett.* **1983**, *1983*, 1047.
(23) Brugger, P. A.; Cuendet, P.; Gratzel, M. *J. Am. Chem. Soc.* **1981**, *103*, 2923.
(24) Reetz, M. T.; Quaiser, S. A.; Breinbauer, R.; Tesche, B. *Angew. Chem., Int. Ed. Engl.* **1995**, *34*, 2728.
(25) Friedrich, K. A.; Henglein, F.; Stimming, U.; Unkauf, W. *Electrochim. Acta* **2001** *47* 689.
(26) Park, S.; Wasileski, S. A.; Weaver, M. J. *J. Phys. Chem. B* **2001**, *105*, 9719.
(27) Park, S.; Tong, Y. Y.; Wieckowski, A.; Weaver, M. J. *Electrochem. Commun.* **2001**, *3*, 509.
(28) Schmidt, T. J.; Gasteiger, H. A.; Staeb, G. D.; Urban, P. M.; Kolb, D. M.; Behm, R. J. *J. Electrochem. Soc.* **1998**, *145*, 2354.
(29) Takasu, Y.; Ohashi, N.; Zhang, X. G.; Murakami, Y.; Minigawa, H.; Sato, S.; Yahikozawa, K. *Electrochim. Acta* **1996**, *41*, 2595.
(30) Yahikozawa, K., Fijii, Y., Matsuda, Y., Nishimura, K., Takasu, Y. *Electrochim. Acta* **1991**, *36*, 973.
(31) Friedrich, K. A.; Henglein, F.; Stimming, U.; Unkauf, W. *Electrochim. Acta* **2000**, *45*, 3283.
(32) Cherstiouk, O. V.; Simonov, P. A.; Savinova, E. R. *Electrochim. Acta* **2003**, *48*, 3851.
(33) Schiffrin, D. J.; Kiely, C. *J. Electroanal. Chem.* **1996**, *409*, 137.
(34) Schiffrin, D. J. *Platinum Met. Rev.* **1999**, *43*, 2.
(35) Paulus, U. A.; Veziridis, Z.; Schnyder, B.; Kuhnke, M.; Scherer, G. G. *J. Electroanal. Chem.* **2003**, *77*, 541.
(36) Kongkanand, A.; Kuwabata, S. *J. Phys. Chem. B* **2005**, *109*, 23190.
(37) Kucernak, A. R.; Chowdhury, P. B.; Wilde, C. P.; Kelsall, G. H.; Zhu, Y. Y.; Williams, D. E. *Electrochim. Acta* **2000**, *45*, 4483.
(38) Antoine, O.; Bultel, Y.; Durand, R. *J. Electroanal. Chem.* **2001**, *499*, 85.
(39) Cherstiouk, O. V.; Simonov, P. A.; Savinova, E. R. *Electrochim. Acta* **2003**, *48*, 3851.
(40) Calandra, P.; Giordano, C.; Longo, A.; Turco Liveri, V. *Mater. Chem. Phys.* **2006**, *98*, 494.
(41) Chen, M.; Cai, Y.; Yan, Z.; Goodman, D. W. *J. Am. Chem. Soc.* **2006**, *128*, 6341.
(42) Stamenkovic, V.; Arenz, M.; Ross, P. N.; Markovic, N. M. *J. Phys. Chem. B* **2004**, *108*, 17915.
(43) Vad, T.; Haubold, H. G.; Waldoefner, N.; Boennemann, H. *J. App. Crystallogr.* **2002**, *35*, 459.
(44) Zhang, J.; Lima, F. H. B.; Shao, M. H.; Sasaki, K.; Wang, J. X.; Hanson, J.; Adzic, R. R. *J. Phys. Chem. B* **2005**, *109*, 22701.
(45) Henry, C. R. *Prog. Surf. Sci.* **2005**, *80*, 92.
(46) Bowker, M.; Stone, P.; Morrall, P.; Smith, Ru.; Bennett, R.; Perkins, N.; Kvon, R.; Pang, C.; Fourre, E.; Hall, M. *J. Catal.* **2005**, *234*, 172.
(47) Gaynutdinov, R.; Vainshtein, D. I.; Hak, S. J.; Tolstikhina, A.; Den Hartog, H. W. *Radiat. Eff. Defects Solids* **2003**, *158*, 77.
(48) Forti, J. C.; Manzo-Robledo, A.; Kokoh, K. B.; De Andrade, A. R.; Alonso-Vante, N. *Electrochim. Acta* **2006**, *51*, 2800.
(49) Rupprechter, G. *Annu. Rep. Prog. Chem., Sect. C: Phys. Chem.* **2004**, *100*, 237.
(50) Lewera, A.; Zhou, W. P.; Vericat, C.; Chung, J. H.; Haasch, R.; Wieckowski, A.; Bagus, P. S. *Electrochim. Acta* **2006**, *51*, 3950.
(51) Colvin, V. L.; Goldstein, A. N.; Alivisatos, A. P. *J. Am. Chem. Soc.* **1992**, *114*, 5221.
(52) Doron, A.; Katz, E.; Willner, I. *Langmuir* **1995**, *11*, 1313.
(53) Chumanov, G.; Sokolov, K.; Gregory, B. W.; Cotton, T. M. *J. Phys. Chem.* **1995**, *99*, 9466.
(54) Teranishi, T.; Hosoe, M.; Miyake, M. *Adv. Mater.* **1997**, *9*, 65.
(55) Roeder, H.; Hahn, E.; Brune, H.; Bucher, J. P.; Kern, K. *Nature* **1993**, *366*, 141.
(56) Bartholomew, C. H.; Boudart, M. *J. Catal.* **1972**, *25*, 173.
(57) Wei, X.; Chen, J.; Yang, L.; Zhaolin, L. *Chem. Commun.* **2002**, 2588.
(58) Zoval, J. V.; Lee, J.; Gorer, S.; Penner, R. M. *J. Phys. Chem. B* **1998**, *102*, 1166.
(59) Liu, H.; Favier, F.; Ng, K.; Zach, M. P.; Penner, R. M. *Electrochim. Acta* **2001**, *47*, 671.
(60) Cortie, M. B.; Van der Lingen, E. *Mater. Forum* **2002**, *26*, 1.
(61) Kuhn, H.; Koch, J.; Hergenroeder, R.; Niemax, K.; Kalberer, M.; Guenther, D. *J. Anal. At. Spectrom.* **2005**, *20*, 894.
(62) Barbara, P. F. *Acc. Chem. Res.* **2005**, *38*, 503 and references therein.
(63) Engelkamp, H.; Hatzakis, N. S.; Hofkens, J.; De Schryver, F. C.; Nolte, R. J. M.; Rowan, A. E. *Chem. Commun.* **2006**, 935.
(64) Meier, J.; Friedrich, K. A.; Stimming, U. *Faraday Discuss.* **2002**, *121*, 365−372.
(65) Meier, J.; Schiot, J.; Liu, P.; Norskov, J. K.; Stimming, U. *Chem. Phys. Lett.* **2004**, *390*, 440.
(66) Eikerling, M.; Meier, J.; Stimming, U. *Z. Phys. Chem.* **2003**, *217*, 395.
(67) Chen, S.; Kucernak, A. *J. Phys. Chem. B* **2004**, *108*, 13984.
(68) Chen, S.; Kucernak, A. *J. Phys. Chem. B* **2003**, *107*, 8392.
(69) Kolb, D. M.; Ullmann, R.; Will, T. *Science* **1997**, *275*, 1097.
(70) Kauffman, G. B. *Inorg. Synth.* **1963**, *7*, 249.
(71) Frens, G. *Nature* **1973**, *241*, 20.
(72) Ahmadi, T. S.; Wang, Z. L.; Green, T. C.; Henglein, A.; El-Sayed, M. A. *Science* **1996**, *272*, 1924.
(73) Xiaolin, N.; Zhennan, G.; Zhongfan, L. *J. Colloid. Interface Sci.* **2002**, *245*, 311.
(74) Penner, R. M. *J. Phys. Chem. B* **2001**, *105*, 8672.
(75) Scharifker, B. R.; Mostany, J. In *Interfacial Kinetics and Mass Transport*; Bard, A. J., Stratmann, M., Calvo, E. J., Eds.; Encyclopedia of Electrochemistry 2; Wiley-VCH: Weinheim, Germany, 2002; p 512.
(76) Tel-Vered, R.; Walsh, D. A.; Mehrgardi, M. A.; Bard, A. J. *Anal. Chem.* **2006**, *78*, 6959.
(77) Serruya, A.; Mostany, J.; Scharifker, B. R. *Faraday. Trans.* **1993**, *89*, 255.
(78) Mandler, D. In *Scanning Electrochemical Microscopy*; Bard, A. J.; Mirkin, M. V., Eds. Marcel Dekker: New York, 2001; p 593.
(79) Bard, A. J.; Faulkner, L. R. *Electrochemical Methods: Fundamentals and Applications*, 2nd ed.; Wiley: New York, 2001; p 216.
(80) Walsh, D. A.; Fernandez, J. L.; Mauzeroll, J.; Bard, A. J. *Anal. Chem.* **2005**, *77*, 5182.
(81) Lee, A.; Bard, A. J. *Anal. Chem.* **2002**, *74*, 3626.
(82) Chen, S.; Kucernak, A. *J. Phys. Chem. B* **2004**, *108*, 3262.
(83) Wipf, D. O.; Bard, A. J. *J. Electrochem. Soc.* **1991**, *138*, 469.
(84) Wipf, D. O.; Bard, A. J. *J. Electrochem. Soc.* **1991**, *138*, L4−L6.
(85) Belqat, B.; Laghzizil, A.; Elkacimi, K.; Bouhaouss, A.; Belcadi, S. *J. Fluorine Chem.* **2000**, *105*, 1.
(86) Kozlowski, C.; Sherwood, P. M. A. *Carbon* **1987**, *25*, 751.
(87) Fitzer, E.; Geigl, K. H.; Huttner, W.; Weiss, R. *Carbon* **1980**, *18*, 265.
(88) Boehm, H.-P.; Diehl, E.; Heck, W.; Sappok, R. *Angew. Chem., Int. Ed. Engl.* **1964**, *3*, 669.
(89) De-Yin, W.; Bin, R.; Yu-Xiong, J.; Xin, X.; Zhong-Qun, T. *J. Phys. Chem. A* **2002**, *106*, 9042.